European Journal of Medicinal Chemistry xxx (xxxx) xxx

Contents lists available at ScienceDirect

European Journal of Medicinal Chemistry

journal homepage: http://www.elsevier.com/locate/ejmech

Design, synthesis and bioevaluation of inhibitors targeting HSP90-CDC37 protein-protein interaction based on a hydrophobic core

Qiuyue Zhang [a, b, 1], Xuexuan Wu [a, b, 1], Jianrui Zhou [a, b], Lixiao Zhang [a, b], Xiaoli Xu [a, b], Lianshan Zhang [c, **], Qidong You [a, b, ***], Lei Wang [a, b, *]

[a] State Key Laboratory of Natural Medicines and Jiang Su Key Laboratory of Drug Design and Optimization, China Pharmaceutical University, Nanjing, 210009, China
[b] Department of Medicinal Chemistry, School of Pharmacy, China Pharmaceutical University, Nanjing, 210009, China
[c] Shanghai Hengrui Pharmaceutical Co., Ltd., Shanghai, 200245, China

ARTICLE INFO

Article history:
Received 24 September 2020
Received in revised form
15 October 2020
Accepted 19 October 2020
Available online xxx

Keywords:
HSP90-CDC37
Protein-protein interaction inhibitors
Anti-proliferation activity
Kinase maturation

ABSTRACT

HSP90-CDC37 protein-protein interaction (PPI) works as a kinase specific-molecular chaperone system to regulate the maturation of kinases. Currently, selectively disrupting HSP90-CDC37 PPI, rather than the direct inhibition of the ATPase function of HSP90, is emerging as a promising strategy for cancer therapy by specifically blocking the maturation of kinases. However, due to the limited understanding of HSP90-CDC37 binding interface, design of small molecule inhibitors targeting HSP90-CDC37 PPI is challenging. In this work, based on the binding mode of **compound 11** (previously reported by our group), we discovered a hydrophobic pocket centered on Phe213, which was previously unknown, contributing to the binding affinity of HSP90-CDC37 PPI inhibitors. A series of hydrophobic substituted inhibitors were utilized to confirm the importance of Phe213 hydrophobic core. Finally, we obtained an optimum compound **DDO-5994** (exhibited an ideal binding pattern on hydrophobic core) with improved binding affinity (K_D = 5.52 μM) and antiproliferative activity (IC_{50} = 6.34 μM). Both *in vitro* and *in vivo* assays confirmed **DDO-5994** as a promising inhibitor to exhibit ideal antitumor efficacy through blocking HSP90-CDC37 PPI.

© 2020 Elsevier Masson SAS. All rights reserved.

1. Introduction

Molecular chaperone heat shock protein 90 (HSP90) is a member of heat shock protein family which plays a pivotal role in physiological function of cells, including cell growth, differentiation and survival [1–3]. At present, more than 200 proteins are found to be client proteins of HSP90, which are maturated with the help of HSP90 [4]. The maturation of kinases is a huge project that completed by HSP90 and many co-chaperones, including CDC37 (cell division cycle 37) [5–8], PP5 (protein phosphatase 5) [9–11], HSP40 [12], HSP70 [12,13], AHA1 (activator of HSP90 ATPase protein 1) and p23 [14]. Among them, CDC37 is a kinase-specific co-chaperone, playing as a hunter in HSP90-CDC37-kinase chaperone cycle for kinase's recruitment and assisting HSP90 to realize the chaperone function [15–17]. In the HSP90-CDC37-kinase chaperone cycle, CDC37 firstly distinguishes and binds to unfolded kinases after phosphorylated by CK2 (casein kinase 2), and subsequently conjugates with HSP90 (Fig. 1A). Then, HSP90 undergoes a conformational transformation after ATP binding. Maturated kinase is released finally after PP5 combines with the above complex and dephosphorylates *p*-CDC37. For the past decade, considering the fundamental role of HSP90 in cancer, HSP90 was regarded as a target for cancer therapy and the main attention was focused on the inhibition of ATPase activity of HSP90 to hinder the kinase maturation [18].

Inhibitors targeting HSP90 ATPase were designed by imitating ATP to occupy the ATP pocket on HSP90, impairing the chaperone function of HSP90 totally [19]. The study of HSP90 ATPase inhibitors kicked off since the discovery of geldanamycin (GA), the first

* Corresponding author. State Key Laboratory of Natural Medicines and Jiang Su Key Laboratory of Drug Design and Optimization, China Pharmaceutical University, Nanjing, 210009, China.
** Corresponding author.
*** Corresponding author. State Key Laboratory of Natural Medicines and Jiang Su Key Laboratory of Drug Design and Optimization, China Pharmaceutical University, Nanjing, 210009, China.
E-mail addresses: youqd@163.com (Q. You), leiwang.91@cpu.edu.cn (L. Wang).
[1] These authors contributed equally.

https://doi.org/10.1016/j.ejmech.2020.112959
0223-5234/© 2020 Elsevier Masson SAS. All rights reserved.

Please cite this article as: Q. Zhang, X. Wu, J. Zhou *et al.*, Design, synthesis and bioevaluation of inhibitors targeting HSP90-CDC37 protein-protein interaction based on a hydrophobic core, European Journal of Medicinal Chemistry, https://doi.org/10.1016/j.ejmech.2020.112959

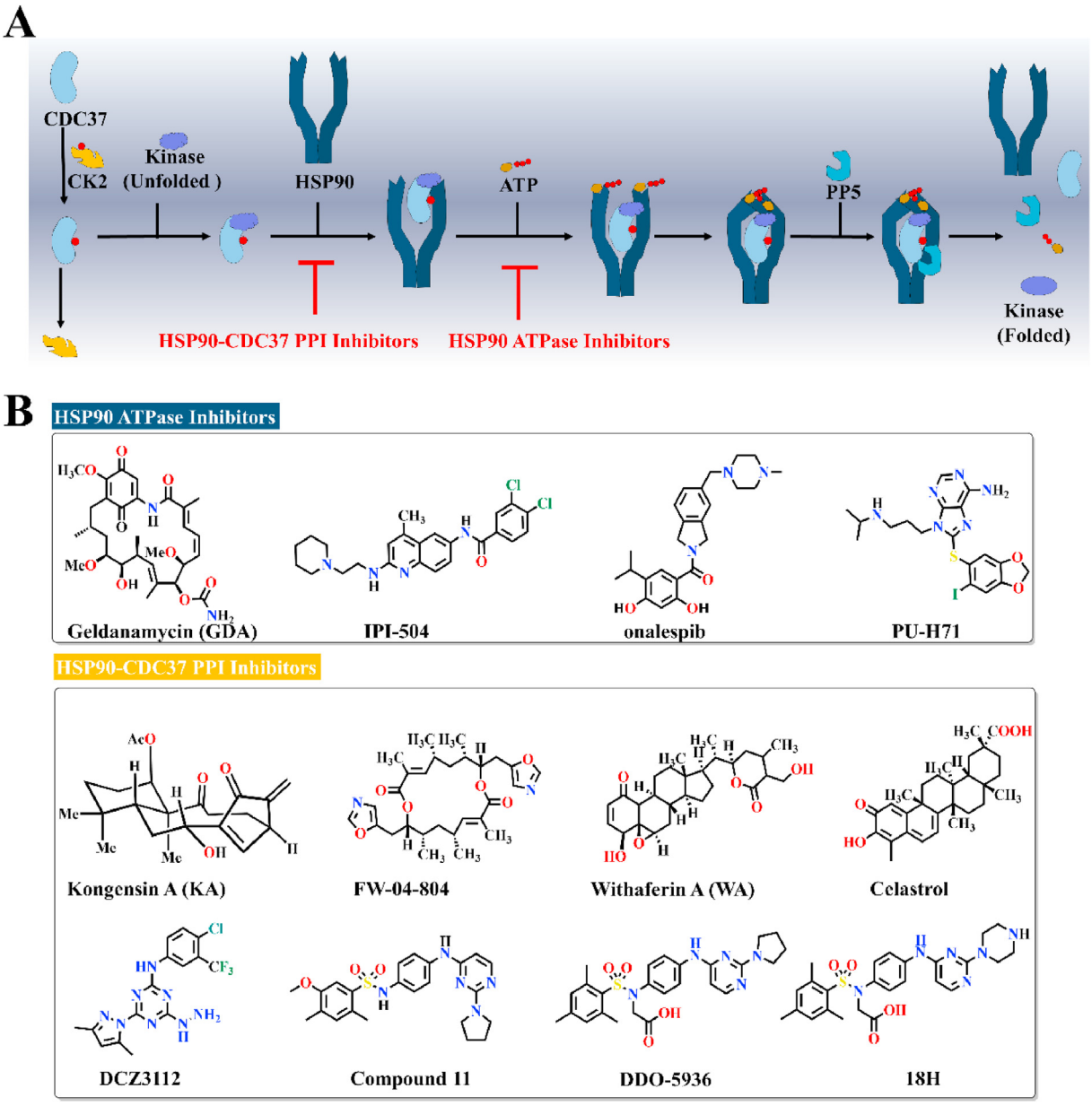

Fig. 1. CDC37-HSP90 PPI plays an important role in kinase maturation and targeting CDC37-HSP90 PPI is a promising strategy for cancer therapy. (A) HSP90-CDC37-kinase chaperone cycle. CDC37 firstly distinguishes and binds to unfolded kinases after phosphorylated by CK2, and subsequently conjugates with HSP90. Then, HSP90 undergoes a conformational transformation after ATP binding. Maturated kinase is released finally after that PP5 combined with the above complex and dephosphorylated CDC37. (B) Representative compounds involving HSP90 ATPase inhibition and HSP90-CDC37 inhibition.

natural product of HSP90 ATPase inhibitor [20]. Up to date, more than 30 HSP90 ATPase inhibitors (including IP-504, onalespib, PU-H71) were entered into clinical trials and most of them were stagnant due to the various inevitable side effects or unsatisfied efficacy, including liver toxicity, heat shock response, high mortality rate, low bioavailability and poor solubility [18,21–23]. Due to multiple downstream pathways (such as CDK4/6 (cyclin dependent kinase4/6), FGFR1 (fibroblast growth factor receptor 1), JAK1 (janus kinase 1), CAMKV (caM kinase like vesicle associated), AKT2 (AKT serine/threonine kinase 2) and TK(tyrosine kinase)) were found to be depended on the function of HSP90, targeting HSP90 ATPase lack of specificity which might induce the degradation of all HSP90 clients, contributing to the main reason for the unsatisfied clinical results of HSP90 ATPase inhibitors. Because of the limited development progress of HSP90 ATPase inhibitors, alternative inhibition strategies to target HSP90 chaperone cycle were emerging. In order to achieve the specific inhibition of HSP90 clients, researchers began to develop HSP90-CDC37 PPI inhibitor with no ATPase inhibition for selectively blocking the kinase maturation in recent years [24–28].

Celastrol was the first natural derived product to exhibit HSP90-CDC37 PPI inhibition activity by a covalently binding mechanism to CDC37 [27]. Afterward, many other natural derived products were discovered with covalent binding mechanism (including Withaferin A (WA), FW-04-806 and Kongensin A (KA)) [29–31]. With the help of crystal structure of HSP90-CDC37, firstly reported in 2004, the rational design of small molecular inhibitors targeting HSP90-CDC37 PPI became feasible [32]. However, the research of HSP90 PPI inhibitor stays in a primary stage and few small molecular inhibitors were reported. In 2018, DCZ3112 was reported as

a HSP90-CDC37 PPI inhibitor with ideal antitumor effects, while the unknown binding site of DCZ3112 limited its further development and optimization [33]. In 2019, our group firstly discovered a lead compound (**compound 11**) by a multiple screening strategy targeting the key interaction region between HSP90 and CDC37 (the most critical polar interaction site for HSP90-CDC37 PPI was confirmed as Glu47). Its structural optimization product, **DDO-5936**, was identified as the first small molecule inhibitor of HSP90-CDC37 PPI with distinct binding site (Glu47 on Hsp90) and molecular mechanism [34]. The discovery of **DDO-5936** demonstrated the feasibility of HSP90-CDC37 PPI inhibition as an effective way to block the maturation of kinases. Then, we conducted a preliminary structure-activity relationship study on **DDO-5936** and obtained an optimized compound **18h** as previously reported [35]. In this work, we firstly discovered a hydrophobic pocket centered on Phe213 on HSP90 which was previously unknown and contributed to the binding affinity of HSP90-CDC37 PPI inhibitors. We synthesized a series of hydrophobic substituted inhibitors based on the binding mode of hit **compound 11** to occupy this hydrophobic pocket, which further confirmed the importance of Phe213. Through a structure-based optimization of inhibitors targeting this hydrophobic region, we have found out the main rules in the design of compounds to interact with Phe213 on the hydrophobic core. Finally, our efforts resulted in an optimum compound **DDO-5994** with improved binding affinity ($K_D = 5.52\ \mu M$) and antiproliferative activity ($IC_{50} = 6.34\ \mu M$) by cyclizing linear aliphatic chain and introducing an oxygen atom (compared to hit **compound 11**, $K_D > 20\ \mu M$ and $IC_{50} > 50\ \mu M$). Both *in vitro* and *in vivo* experiments were carried out to confirm the efficacy of **DDO-5994** as a promising HSP90-CDC37 PPI inhibitor. In addition, our results also provided a novel binding site on Phe213 as a hydrophobic core for the further design of HSP90-CDC37 PPI inhibitors.

2. Results and discussion

2.1. Molecular docking and MD simulation revealed a hydrophobic pocket involving Phe213 on HSP90-compound 11 interaction surface

Our previous study discovered hit **compound 11**, which disrupted HSP90-CDC37 PPI moderately through a direct binding manner on HSP90 ($K_D = 21.1\ \mu M$, inhibition rate ~56% at 100 μM) [34]. Based on the binding mode of HSP90-**compound 11**, we performed molecular docking and molecular dynamic (MD) simulation to explore the characters of binding modes during the dynamic trajectory. Besides Glu47, Ser50 and Asn51, which were previously reported as important polar sites for the binding of HSP90-CDC37, energy decomposition revealed a hydrophobic residue, Phe213, also contributed to the main driving force for the interaction between HSP90 and **compound 11**, which was previously unknown (Fig. 2B). This hydrophobic pocket contributed to the majority of hydrophobic forces adjacent to the binding surface of **compound 11** which might be an ideal site for small molecule design. We supposed that occupation of this pocket would enhance the binding affinity between HSP90 and inhibitors by introducing hydrophobic groups. Based on this hypothesis, we divided the structure of **compound 11** into three parts, including A ring (adjacent hydrophobic pocket), sulfamide part, and pyrimidine substituents (forms hydrophilic interaction). In previous studies, by changing pyrrole ring to piperazine ring in pyrimidine substituents (**18h**) and forming hydrochloride, the hydrophilic interaction is greatly improved and the physical properties were also well optimized [35]. Here, our efforts are committed to increase the hydrophobic interactions. Thus, we conserved piperazine ring and focused on A ring by employing hydrophobic substituted groups to occupy the pocket involving Phe213 (Fig. 2C).

2.2. Occupation of hydrophobic pocket lead to optimum compound DDO-5994 with improved binding affinity and antiproliferative activity

We introduced different kinds of hydrophobic substitutions on the A ring to explore the optimal chemical scaffold for the occupation of hydrophobic pocket centered on Phe213, including heterocycles, heteroatoms, aliphatic chains and aromatic rings (Scheme 1). All compounds were determined by BLI (biolayer interferometry assay) and antiproliferation assay firstly. As shown in Table 1, **DDO-5974** and **DDO-5975** loss activity completely, indicating that heterocycles like imidazole ring and thiophene ring are not suitable for this pocket. **DDO-5976~DDO-5980** exhibited no binding affinity by BLI assay, indicating that halogen heteroatom substitutions and cyano group are not suitable for this region either. Subsequent result revealed **DDO-5981** ($K_D = 18.4\ \mu M$, $IC_{50} = 13.7\ \mu M$) and **DDO-5982** ($K_D = 11.5\ \mu M$, $IC_{50} = 19.3\ \mu M$) with moderate binding affinity and antiproliferative activity. The binding mode of **DDO-5981**($K_{off} = 0.112\ s^{-1}$) showed that biphenyl substitution could not entirely enter the hydrophobic pocket because of the structural rigidity, accounting for the more rapid dissociation rate comparing with **DDO-5982** ($K_{off} = 0.0366\ s^{-1}$, Fig. 3A and D). MD simulation revealed that the non-polar interaction with Phe213 was enhanced but the polar interactions between **DDO-5981** and HSP90 were reduced sharply (interaction with Glu47, Ser50, Asn51), which accounted for the limitation of the K_D value (Fig. 3B, C, 3D). **DDO-5982** with propyl substitution exhibited similar binding mode with the above compound (Fig. 3A). MD simulation shows that **DDO-5982** exhibited no strong interaction with key residue (Glu47, Ser50, Asn51, Phe213), which implied that there is still capacity to be occupied (Fig. 3B and C).

Based on the above results, we subsequently changed benzene rings into phenyl ether (**DDO-5983**) or benzyl ether (**DDO-5984**) to reduce the structural rigidity for enhanced binding affinity. Disappointingly, **DDO-5983** and **DDO-5984** lost binding affinity completely as shown in Table 2. Above results suggested that it might be too large for biphenyl substitution to enter the hydrophobic pocket properly. Next, we explored how long and which type of aliphatic chain could match the hydrophobic pocket appropriately. As shown in Table 2, substitutions with 1—5 carbon aliphatic chain were synthesized and C4 (**DDO-5988**) showed better binding affinity and antiproliferative activity. Compared the compounds with branched chains (**DDO-5987**, **DDO-5991**, $K_D > 100\ \mu M$ or NA, $IC_{50} > 20$ or NA), the compound substituted with linear chain (**DDO-5982**) exhibited advantages on binding affinity and antiproliferative activity ($K_D = 11.5\ \mu M$, $IC_{50} = 19.3\ \mu M$). Thus, we introduced an ester group with four atoms in the main chain (**DDO-5990**, $K_D = 5.13\ \mu M$,$K_{on} = 3.55 \times 10^4\ Ms^{-1}$) and it exhibited improved binding affinity compared to **DDO-5988** ($K_D = 11.6\ \mu M$,$K_{on} = 1.04 \times 10^4\ Ms^{-1}$) with more rapid association rate. Molecular docking and MD simulation show that the ester group enters the hydrophobic pocket deeply and forms a strong hydrophobic interaction with Phe213. However, the binding pattern of **DDO-5990** changed the conformation of skeleton, resulting in the loss of binding energy with Glu47 (Fig. 3A, B, 3C). So far, all the results show that the four atoms length is the most suitable for the hydrophobic pocket and the ester group may be beneficial to enhance the binding affinity.

In order to prevent the conformational change of **DDO-5990**, we converted linear chain into loop to reduce the entropy loss. We designed and synthesized **DDO-5992~DDO-5994** by cyclization to decrease the flexibility of *n*-butyl. As shown in Table 3, **DDO-5994** showed the optimal results both in binding affinity and antiproliferation activity ($K_D = 5.52\ \mu M$, $IC_{50} = 6.34\ \mu M$). According to the results of molecular docking and molecular dynamic simulation

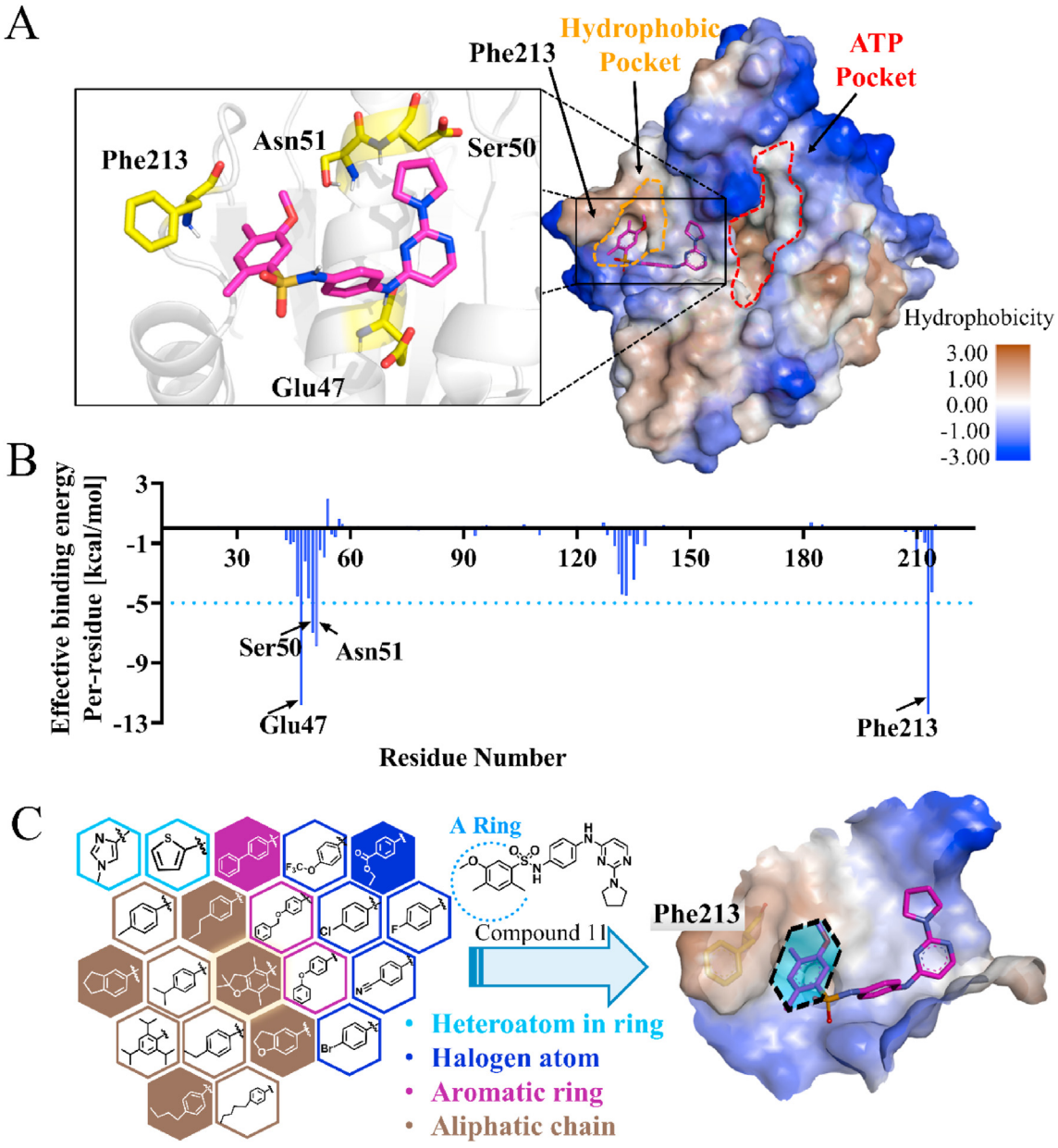

Fig. 2. Binding mode analysis of HSP90-Compound 11 and design of hydrophobic substituted derivatives. (A) Binding mode of **compound 11**. (B) Energy decomposition of Hsp90-**compound 11** interaction. (C) Optimization strategies and compound design.

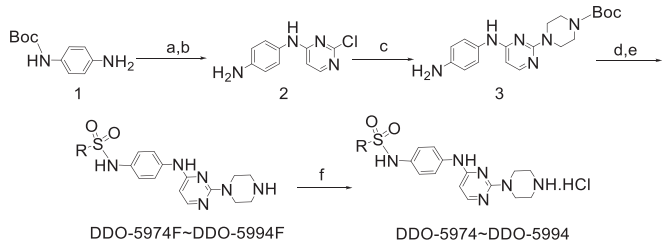

Scheme 1. Synthetic route of compounds DDO-5974~DDO-5994. Reagents and conditions: (a). 2,4-Dichloropyrimidine, *i*-PrOH, TEA, reflux; (b). TFA, DCM, rt.; (c). 1-Boc-piperazine, DMF, K_2CO_3, 100 °C; (d). Substituted benzenesulfonyl chloride, DCM, TEA, rt; (e). 36% HCl aqueous, EA, rt. (f). 1 M isopropanol hydrochloride solution, EA, rt.

(Fig. 3), **DDO-5994** occupied the hydrophobic pocket in an appropriate posture and formed strong interactions with key residues of HSP90 (Glu47, Ser50, Asn51, Phe213). Comparing with aforementioned compounds, **DDO-5994** interacted with HSP90 more steadily (Fig. S1).

So far, some conclusions have been drawn from the process of hydrophobic occupation. Halogen atoms and heterocycles (like imidazole ring and thiophene ring) are taboos in this pocket, which will lead to the complete loss of activity of compounds; biphenyl substitution is too bulky to fit this pocket; four atoms are the optimum size to occupy the pocket, less than 4 atoms cannot form strong interaction with Phe213, and more than 4 atoms cannot enter the pocket in a proper posture; linear aliphatic chain can

Table 1
SARs of different types of hydrophobic substitutions on A ring.

Entry	Compound	R	K_D (μM)<	K_{on} (1/Ms)	K_{off} (1/s)	IC_{50} (μM)
1	**DDO-5974**		NA	NA	NA	NA
2	**DDO-5975**		NA	NA	NA	>20
3	**DDO-5976**	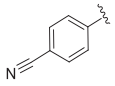	NA	NA	NA	>20
4	**DDO-5977**		NA	NA	NA	>20
5	**DDO-5978**	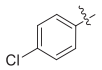	NA	NA	NA	11.1 ± 1.24
6	**DDO-5979**	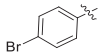	NA	NA	NA	1.35 ± 0.08
7	**DDO-5980**	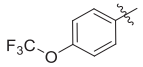	NA	NA	NA	>20
8	**DDO-5981**	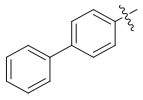	18.4	6.10×10^3	0.112	13.7 ± 1.86
9	**DDO-5982**	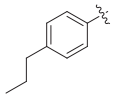	11.5	3.17×10^3	0.0366	19.3 ± 4.85

cause a great change in the conformation of compounds and reduce the key polar interaction with Glu47 sharply. According to the above process, we obtained the optimum compound **DDO-5994** with moderate binding affinity ($K_D = 5.52$ μM) and antiproliferative activity ($IC_{50} = 6.34$ μM).

2.3. DDO-5994 directly bound to Hsp90 and efficiently disrupted HSP90-CDC37 PPI in cells and induced kinase degradation

To confirm the mechanism of **DDO-5994**, we firstly conducted a cellular thermal shift assay (CESTA) to determine the binding affinity in cells. As shown in Fig. 4A, with the treatment of 5 μM **DDO-5994** or DMSO for 12 h in HCT116 cells with temperature ranging from 35 to 65 °C, **DDO-5994** could stabilize HSP90 rather than CDC37 under the high temperature environment by Western blot (WB) analysis, indicating a direct binding manner of **DDO-5994** to HSP90 in cells. Subsequently, we operated a co-immunoprecipitation (co-IP) assay to determine the ability of **DDO-5994** as a HSP90-CDC37 PPI inhibitor. As shown in Fig. 4B, after the treatment with **DDO-5994** (0, 1, 5, and 10 μM) in HCT116 cells, we immunoprecipitated Hsp90 to detect the bait proteins. It was clearly observed that **DDO-5994** disrupt HSP90-CDC37 PPI in a concentration-dependent manner by quantitative analysis. Because of the block of HSP90-CDC37 PPI, CDK4, a representative kinase client protein of HSP90 was decreased as expected (Fig. 4B).

To further investigate the effect of **DDO-5994** to the downstream kinases of HSP90, we carried out Western blot experiments to determine the representative client proteins of HSP90-CDC37. As shown in Fig. 4C, kinase clients of HSP90 including CDK4 and CDK6, were down-regulated significantly by **DDO-5994** in a concentration-dependent manner, which led to the down-regulation of cyclin D1 and the upregulation of p21/p27. Similar with our previous results, HSP70 was remained on a constant level which indicated to no risk of potential heat shock reaction (HSR). All the above results indicated that **DDO-5994** directly bound to HSP90 and efficiently disrupted HSP90-CDC37 PPI in cells and induced kinase degradation.

2.4. DDO-5994-induced cell cycle arrest

The clients of Hsp90-Cdc37, CDK4 and CDK6, play important roles in cell cycle process [36–38]. Based on the above results (Fig. 4), we subsequently conducted a cell cycle distribution analysis following a standard flow cytometry method. HCT116 cells were treated with **DDO-5994** in different concentrations (0, 1, 5, and 10 μM) for 24 h and the DNA was stained with propidium iodide. As shown in Fig. 5, the proportion of HCT116 cells in G_0/G_1 phase was increased after the treatment of **DDO-5994**, which indicating that **DDO-5994** could inhibit cell cycle progression by arresting in G_0/G_1 phase.

2.5. DDO-5994 exhibits potency and safety in vivo

As shown in Fig. 6, we evaluated the antitumor efficacy of **DDO-5994** in mice bearing HCT116 xenografts tumors. **DDO-5994** and **18h** were administrated daily for 37 days at 10 mg/kg and 20 mg/kg,

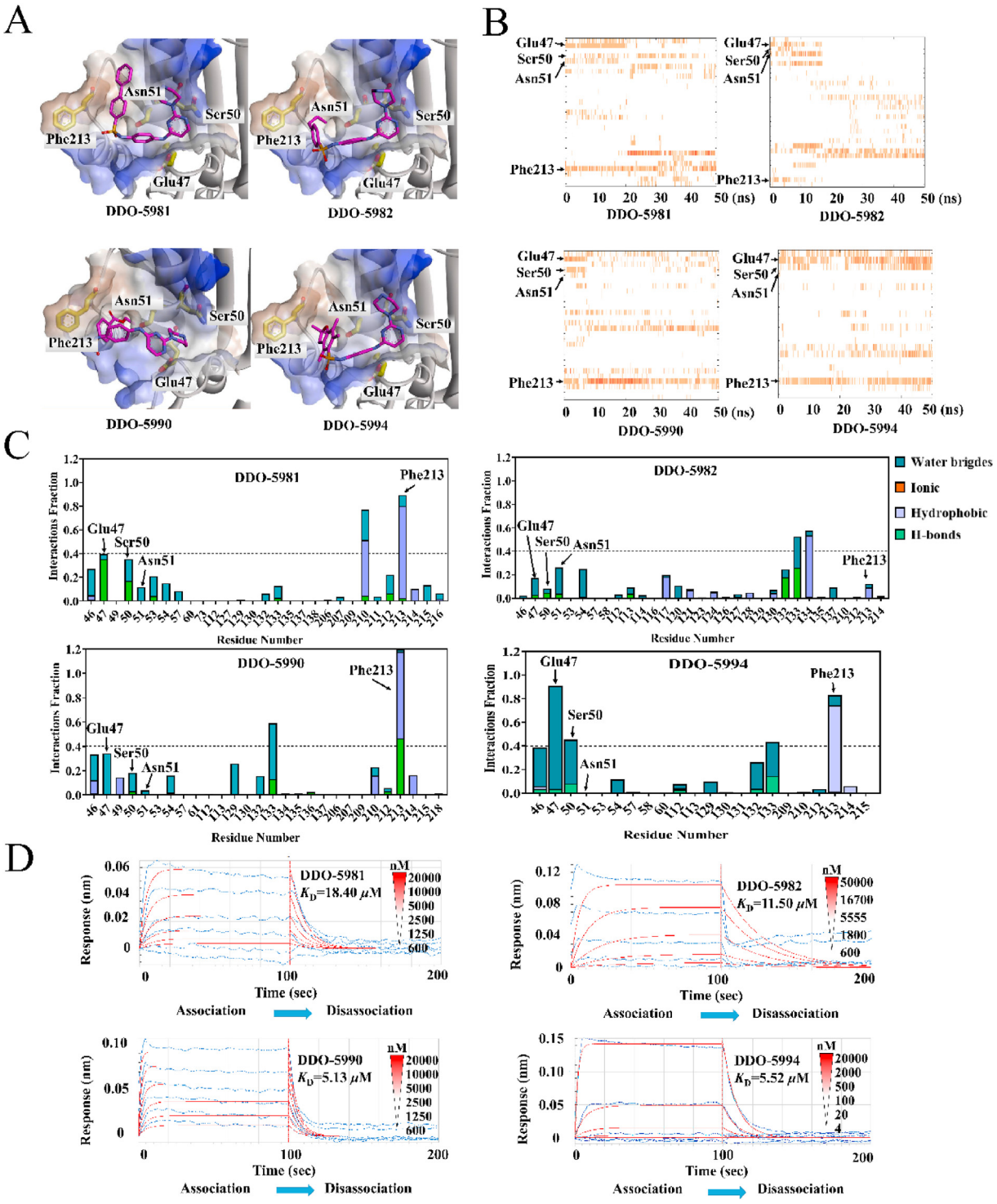

Fig. 3. Overview of the interactions and binding affinities between key compounds and HSP90. (A) Predicted binding modes of key compounds by molecular docking. (B) Timeline representation of the interactions and contacts (H-bonds, Hydrophobic, Ionic, Water bridges). (C) Simulation Interactions Diagram. Protein-ligand interactions are categorized into four types: Hydrogen Bonds, Hydrophobic, Ionic and Water Bridges. (D) Binding affinity of key compounds with HSP90 protein, determined by binding kinetic assay of biolayer interferometry (ForteBio Octet).

respectively. **DDO-5994** and **18h** were both tolerated with no weight loss (Fig. 6A). **DDO-5994** inhibited the growth of tumor in a dose-dependent manner and exhibited increasing potency than **18h** in the high dose group, which was characterized by tumor volume and weight. The result of antitumor efficacy experiment was consistence with the data reported previously [35]. Hematoxylin eosin (H&E) staining analysis showed consistent results and confirmed that **DDO-5994** exhibited *in vivo* anti-proliferation efficacy (Fig. 6D). Compared to the group of **18h**, CDK4 was observably decreased in **DDO-5994** group with a dose-dependent manner indicated by immunohistochemical staining. In brief, **DDO-5994** was proved a better HSP90-CDC37 PPI inhibitor

Table 2
SARs of different types of biphenyl and aliphatic chains substitutions on A ring.

Entry	Compound	R	K_D (μM)	K_{on} (1/Ms)	K_{off} (1/s)	IC_{50} (μM)
1	**DDO-5983**	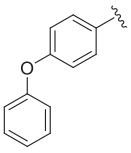	NA	NA	NA	>20
2	**DDO-5984**	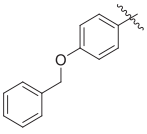	NA	NA	NA	7.05 ± 1.20
3	**DDO-5985**		NA	NA	NA	>20
4	**DDO-5986**	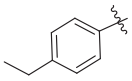	NA	NA	NA	>20
5	**DDO-5987**	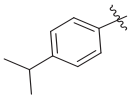	>100	–	–	>20
6	**DDO-5988**	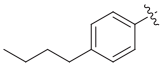	11.6	1.04×10^4	0.121	7.50 ± 1.60
7	**DDO-5989**	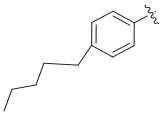	>100	–	–	16.7 ± 2.73
8	**DDO-5990**	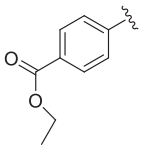	5.13	3.55×10^4	0.182	16.4 ± 3.15
9	**DDO-5991**	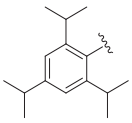	NA	NA	NA	>20

with more potent antitumor efficacy and good tolerance by the introduction of hydrophobic substituted groups.

3. Conclusions

PPIs play important roles in the function of cells. Specific modulation of PPIs is a promising strategy to regulate the function of cells preciously and achieve therapy goals. HSP90-CDC37 PPI plays a key role in the maturation of kinases that related to cancer closely. Comparing with HSP90 ATPase inhibitor, HSP90-CDC37 PPI inhibitor has more specificity to avoid side effects like HSR. In this study, we discovered a hydrophobic pocket centered on Phe213 based on HSP90-**compound 11** binding mode by molecular docking and MD simulation. Phe213 was previously unknown and contributed to the binding affinity of HSP90-CDC37 PPI inhibitors. We supposed the hydrophobic pocket where Phe213 located was a breakthrough to improve binding affinity and antiproliferative efficacy. We introduced diverse type of hydrophobic groups to A ring of **compound 11** to enhance hydrophobic interaction between compound and HSP90 and constantly adjusted the optimization strategy according to real-time results. Some rules were revealed by adapting the hydrophobic pockets with diverse hydrophobic groups. Halogen atoms and heterocycles (like imidazole ring and thiophene ring) are taboos in this pocket, which will lead to the complete loss of activity of compounds; biphenyl substitution is too bulky to fit this pocket; linear aliphatic chains are more adapted than branch aliphatic chains and four atoms are the optimum size to occupy the pocket, less than 4 atoms cannot form strong interaction with Phe213, and more than 4 atoms cannot enter the pocket in a proper posture; linear aliphatic chain can cause a great change in the conformation of compounds and reduce the key polar interaction with Glu47 sharply; ester group with four atoms in main chain is beneficial to binding affinity. In order to prevent the conformational change of skeleton caused by long linear aliphatic chain, we decreased the flexibility of linear

Table 3
SARs of different types of cyclic aliphatic chain substitutions on A ring.

Entry	Compound	R	K_D (μM)	K_{on} (1/Ms)	K_{off} (1/s)	IC_{50} (μM)
1	**DDO-5992**	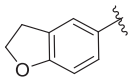	10.6	3.02×10^3	0.0321	5.82 ± 1.08
2	**DDO-5993**	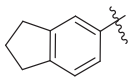	9.52	3.54×10^4	0.337	13.4 ± 3.78
3	**DDO-5994**	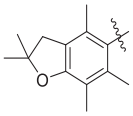	5.52	2.03×10^4	0.112	6.34 ± 2.67
4	**Compound 11**	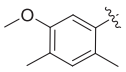	>20	–	–	>50

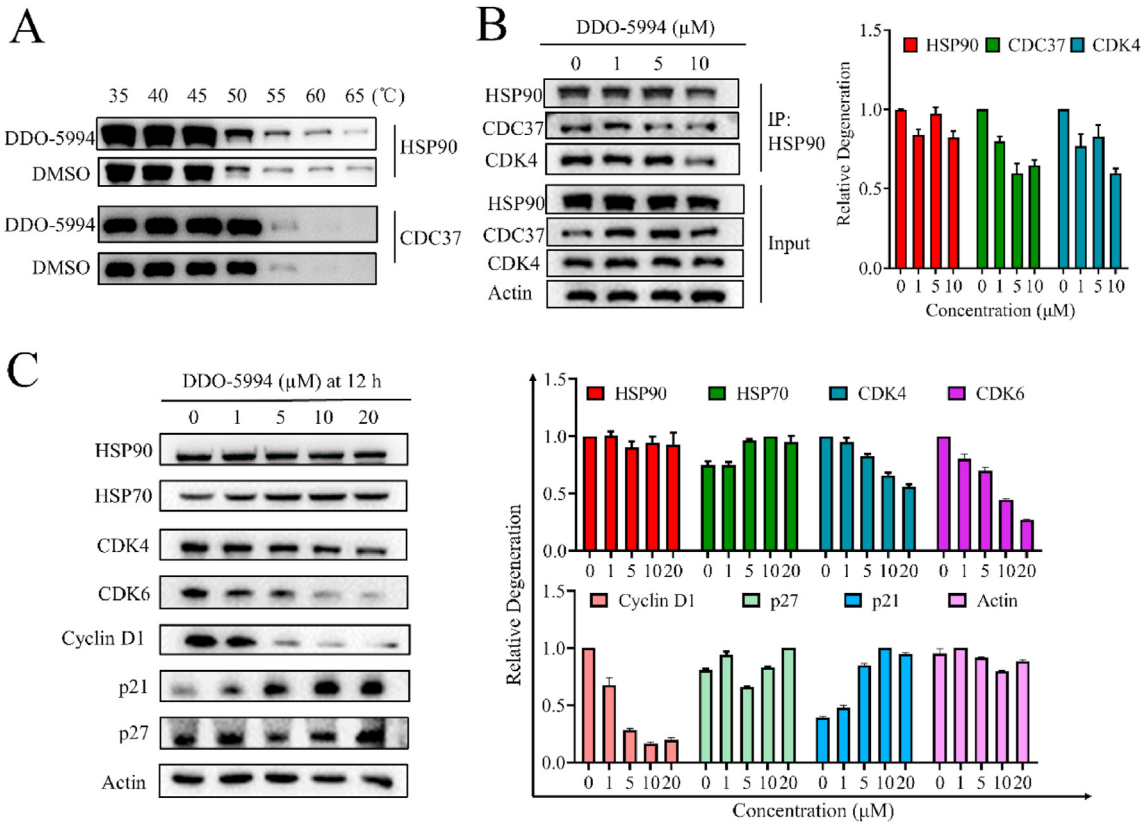

Fig. 4. DDO-5994 disrupted the Hsp90-Cdc37 PPI in cells through directly binding to Hsp90, and down-regulated kinase clients of Hsp90 without HSR. (A). CETSA of HCT116 cells treated with DMSO or 5 μM of **DDO-5994** for 12 h. Data are the representative of three independent experiments. (B). co-IP assay of **DDO-5994** (concentrations of the compound increasing from 0, 1, and 5–10 μM) in HCT116 cells. **DDO-5994** efficiently blocked Hsp90-Cdc37 PPI through a dose-dependent manner, leading to the dissociation of CDK4 from the Hsp90-Cdc37 complex. Western blots were performed with *anti*-Hsp90, *anti*-Cdc37, or *anti*-CDK4 in each experiment. (C). Dose-dependent Western blot analysis of Hsp90, Hsp70, Cdc37, CDK4, CDK6, cyclin D1, p21, and p27 protein expression levels in HCT116 cells after treatment with 0, 1, 5, and 10 μM **DDO-5994** for 12 h. β-Actin was used as a loading control. Data are the representative of three independent experiments.

aliphatic chain by cyclization strategy and introduction of oxygen atom to obtain **DDO-5994** finally. *In vitro* and *in vivo* assays confirmed that **DDO-5994** directly bound to HSP90 and disrupted HSP90-CDC37 interaction, thus to block kinases maturation. **DDO-5994** exhibited antiproliferative activity by down-regulating CDK4/6 to cause cell cycle arrest. *In vivo* assay also revealed **DDO-5994** with improved antiproliferation activity and safety. In this study, it was proved that Phe213 could be regarded as a suitable hydrophobic binding site for the design of small molecule inhibitors targeting HSP90-CDC37 PPI. In addition, **DDO-5994** was achieved with improved *in vivo* efficacy, providing new options for the further design of HSP90-CDC37 inhibitors.

Comparing with HSP90 ATPase inhibitors, HSP90-CDC37 PPI inhibitors exhibit significant advantages in the mechanism with

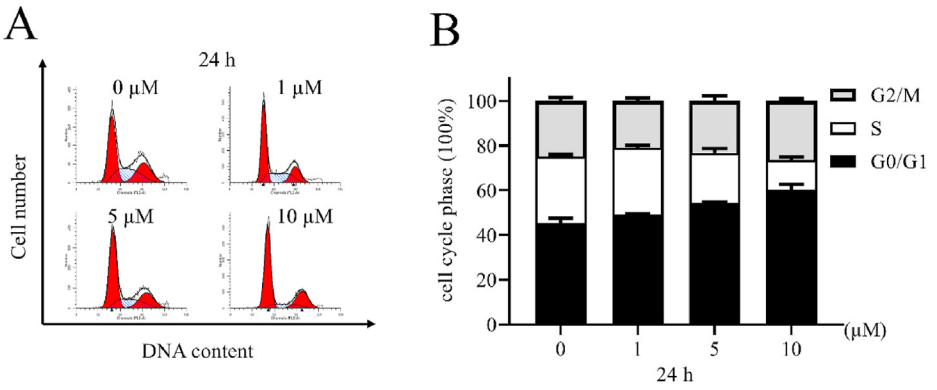

Fig. 5. DDO-5994 induced cell cycle arrest in HCT116 cells. (A) Cell cycle distribution determined by PI staining of HCT116 cells after treatment with 0, 1, 5, and 10 μM of **DDO-5994** for 24 h, respectively. (B) Graphic histogram of cell cycle distribution.

specificity to kinase maturation. The study of HSP90-CDC37 PPI inhibitors is in primary stage and further research may focused on following directions: (1) discovering small molecules directly binding with CDC37 to disrupt HSP90-CDC37 PPI; (2) improving the druggability of existing compounds in terms of physical and chemical properties; (3) HSP90-CDC37 PPI modulators play an important role in the regulation of HSP90-CDC37-kinase cycle and might be used as chemical probes to study the mechanism of HSP90-CDC37 chaperone cycle for kinase recruitment, which help to discovery more efficient HSP90-CDC37 PPI inhibitors for the cancer therapy; (4) with the different mechanism to inhibit kinase, HSP90-CDC37 PPI inhibitors might be used in combination with other kinase inhibitors to achieve more potential cancer therapy effects.

4. Experimental section

4.1. Materials and methods

Unless otherwise mentioned, all of the commercial reagents were reagent grade and directly used without further purification. All the reactions were visualized using UV light at 254 nm and monitored by thin layer chromatography (TLC) on 0.25 mm silica gel plates (GF-2.5). ^{1}H NMR and ^{13}C NMR spectra were tested by Bruker AV300 instrument with tetramethylsilane as the standard to report chemical shifts. ESI-MS and high-resolution mass spectra (HRMS) results of all the compounds were recorded on a Waters Q-Tof micro mass spectrometer (all data were within 0.4% of the theoretical values). The purity (≥95%) of the compounds was determined by the HPLC on a Waters C18 column (4.6 mm × 150 mm, 3.5 μm) using a mixture of solvent containing methanol/methanol with 1‰ TEA at a flow rate of 1.0 mL/min and the peaks were determined at 254 nm under UV. The HPLC chromatograms and ^{1}H NMR, ^{13}C NMR and HRMS spectra of the new compounds are presented in supporting information.

4.2. Chemistry

4.2.1. N^1-(2-chloropyrimidin-4-yl)benzene-1,4-diamine (**2**)

Tert-butyl (4-aminophenyl)carbamate (5.0 g, 24.0 mmol), 2,4-dichloropyrimidine (7.2 g, 48.3 mmol) were dissolved in *i*-PrOH (80 ml), followed by TEA (13 ml, 93.8 mmol). The mixture was reflux overnight. After completion of the reaction, the mixture was cool to room temperature and solvent was removed by evaporation under reduce pressure. Then ethyl acetate (50 ml) was added to residues and stirred in room temperature for 30 min. Filtered and the solvent was evaporated under reduce pressure to give crude product. The crude product purified by silica gel chromatography (PE-EA, 4:1), yielding *tert*-butyl (4-((2-chloropyrimidin-4-yl) amino)phenyl)carbamate as light yellow solid (6.6 g, 85%). *tert*-butyl (4-((2-chloropyrimidin-4-yl)amino)phenyl)carbamate (10 g, 31.2 mmol) was dissolved in DCM(60 ml) followed by TFA (20 ml). The mixture was stirred at room temperature for 4 h. Then saturated $NaHCO_3$ aqueous was added to adjust the pH to 8–9. Collected organic layer and dry over anhydrous Na_2SO_4 and evaporated under reduce pressure to give compound **2** as off-white solid (6.8 g, 99%).^{1}H NMR (300 MHz, DMSO-d_6) δ 9.63 (s, 1H), 8.02 (d, J = 5.9 Hz, 1H), 7.23–7.05 (m, 2H), 6.65 (d, J = 8.7 Hz, 2H), 6.54 (d, J = 6.0 Hz, 1H). HRMS (ESI): found 221.05887 ($C_{10}H_9ClN_4$ $[M + H]^+$, requires 221.05885).

4.2.2. Tert-butyl 4-(4-((4-aminophenyl)amino)pyrimidin-2-yl) piperazine-1-carboxylate (**3**)

Compound **2** (3.5 g, 15.9 mmol), 1-Boc-piperazine (3.5 g, 18.8 mmol) were dissolved in dry DMF (20 ml) followed by dry K_2CO_3 (4.38 g, 31.7 mmol). The reaction mixture was stirred at 100 °C under nitrogen gas for overnight. After completion of the reaction, the mixture was cool to room temperature and water (230 ml) was added to the mixture by drops to precipitate the product. Filtered and cake was dried in a vacuum desiccator before washed with water (20 ml). Compound **3** was afforded as purple brown solid (5.8 g, 98%). ^{1}H NMR (300 MHz, DMSO-d_6) δ 8.78 (s, 1H), 7.84 (d, J = 5.7 Hz, 1H), 7.17 (d, J = 8.1 Hz, 2H), 6.56 (dd, J = 8.7 Hz, 2H), 5.90 (d, J = 5.8 Hz, 1H), 4.89 (s, 2H), 3.66 (dd, J = 6.9, 3.7 Hz, 4H), 3.39 (dd, J = 7.2 Hz, 4H), 1.45 (s, 9H). HRMS (ESI): found 371.22013 ($C_{19}H_{26}N_6O_2$ $[M + H]^+$, requires 371.219).

4.2.3. General procedure for the preparation of compounds ***DDO-5974~DDO-5994***

Compound **3** (350 mg, 0.9 mmol), TEA (0.025 ml, 1.8 mmol) were dissolved in DCM (15 ml) followed adding substituted benzenesulfonyl chloride (0.8 mmol, dissolved in DCM, 3 ml) by drops at room temperature. The mixture was stirred for overnight and then evaporated under reduce pressure. The crude residue purified by silica gel chromatography (PE-EA, 4:1). Compound with Boc group was obtained as light yellow solid and then was dissolved in EA (20 ml) followed by adding 36% HCl aqueous (4 ml). The mixture was stirred at room temperature for 2 h and solvent was adjusted to pH = 7–8 by saturated sodium bicarbonate solution. Organic layer was dried by anhydrous sodium sulfate and evaporated under reduce press to get free compounds. Then free compound was dissolved in EA followed 1 M isopropanol hydrochloride solution (1 eq) at room temperature for 1 h. The residue crystalized from EA to give **DDO-5974~DDO-5994** finally.

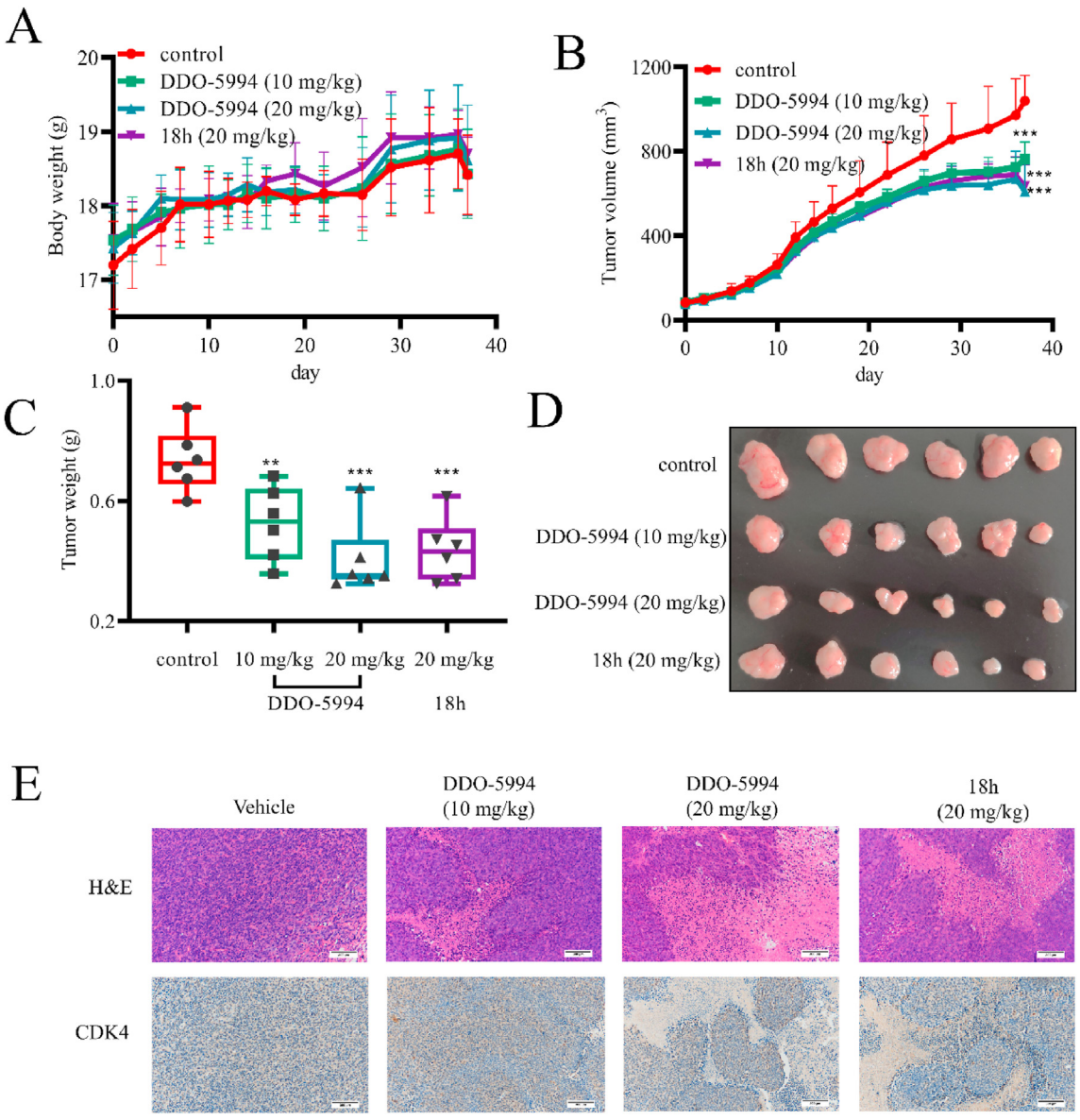

Fig. 6. DDO-5994 dose-dependently impaired the growth of xenografted HCT116 cells in immunocompromised mice and safety *in vivo*. (A) *In vivo* antitumor efficacy of **DDO-5994** and **18h** in the HCT116 xenograft model. Mice were administered with **DDO-5994** (0, 10, and 20 mg/kg, respectively) and **18h** (20 mg/kg) daily by gavage starting 7 days after cell implantation. Effects on body weight changes of the mice treated with **DDO-5994** and **18h**. (B) Tumor volumes were determined by calipers. The tumor volumes are plotted as the mean ± SD. (*$P < 0.05$; **$P < 0.01$; ***$P < 0.001$, $n = 6$). (E) H&E staining showed the tumor tissue morphology of different groups with **DDO-5994** and **18h**. Scale bars were represented as 300 μm. The expression levels of CDK4 were analyzed in tumor tissues by immunohistochemistry.

*4.2.4. Characterization data for final compounds **DDO-5974~DDO-5994***

*4.2.4.1. 1-Methyl-N-(4-((2-(piperazin-1-yl)pyrimidin-4-yl)amino) phenyl)-1H-imidazole-4-sulfonamide hydrochloride (**DDO-5974**).* It was obtained in 35% yield as off-white solid; ^{1}H NMR (300 MHz, DMSO-d_6) δ 11.19 (s, 1H), 10.27 (s, 1H), 9.69 (s, 3H), 7.86 (d, J = 7.1 Hz, 1H), 7.82 (s, 1H), 7.77 (s, 1H), 7.53 (d, J = 7.0 Hz, 4H), 7.19 (d, J = 8.6 Hz, 3H), 6.54 (s, 1H), 4.03 (t, J = 4.7 Hz, 4H), 3.66 (s, 4H), 3.25 (s, 8H). HRMS (ESI): found 415.16595 ($C_{18}H_{22}N_8O_2S$ [M + H]$^+$, requires 415.16592).

*4.2.4.2. N-(4-((2-(piperazin-1-yl)pyrimidin-4-yl)amino)phenyl)thiophene-2-sulfonamide hydrochloride (**DDO-5975**).* It was obtained in 36% yield as off-white solid;^{1}H NMR (300 MHz, DMSO-d_6) δ 9.15 (s, 1H), 7.87 (d, J = 5.6 Hz, 1H), 7.70 (d, J = 8.9 Hz, 2H), 7.53–7.37 (m, 4H), 7.23 (t, J = 7.4 Hz, 1H), 7.11–6.97 (m, 6H), 5.95 (d, J = 5.6 Hz, 1H), 3.58 (d, J = 5.0 Hz, 4H), 2.71 (t, J = 5.0 Hz, 4H). HRMS (ESI): found 503.18567 ($C_{26}H_{27}N_6O_3S$ [M + H]$^+$, requires 503.18599).

*4.2.4.3. 4-Cyano-N-(4-((2-(piperazin-1-yl)pyrimidin-4-yl)amino) phenyl) benzenesulfonamide hydrochloride (**DDO-5976**).* It was obtained in 33% yield as off-white solid;^{1}H NMR (300 MHz, DMSO-d_6) δ 9.16 (s, 1H), 8.01 (d, J = 8.5 Hz, 2H), 7.93–7.77 (m, 3H), 7.46 (d, J = 8.9 Hz, 2H), 6.97 (d, J = 8.9 Hz, 2H), 5.97 (d, J = 5.7 Hz, 1H), 3.62 (t, J = 5.0 Hz, 4H), 2.78 (d, J = 5.0 Hz, 4H). HRMS (ESI): found 436.15469 ($C_{21}H_{21}N_7O_2S$ [M + H]$^+$, requires 436.15502).

*4.2.4.4. 4-Fluoro-N-(4-((2-(piperazin-1-yl)pyrimidin-4-yl)amino) phenyl) benzenesulfonamide hydrochloride (**DDO-5977**).* It was obtained in 38% yield as off-white solid; ^{1}H NMR (300 MHz, DMSO-d_6) δ 11.04 (s, 1H), 10.41 (s, 1H), 9.59 (s, 2H), 7.89 (d, J = 6.8 Hz, 1H), 7.86–7.74 (m, 2H), 7.55 (d, J = 8.0 Hz, 3H), 7.47–7.36 (m, 2H), 7.15 (d,

J = 8.9 Hz, 2H), 6.49 (d, J = 6.8 Hz, 1H), 4.00 (t, J = 5.2 Hz, 4H), 3.24 (s, 4H). HRMS (ESI): found 429.15058 ($C_{20}H_{21}FN_6O_2S$ [M + H]$^+$, requires 429.15035).

*4.2.4.5. 4-Chloro-N-(4-((2-(piperazin-1-yl)pyrimidin-4-yl)amino) phenyl) benzenesulfonamide hydrochloride (**DDO-5978**).* It was obtained in 36% yield as off-white solid; ^{1}H NMR (300 MHz, DMSO-d_6) δ 10.46 (s, 1H), 9.56 (s, 2H), 7.89 (d, J = 6.8 Hz, 1H), 7.75 (d, J = 8.7 Hz, 2H), 7.64 (d, J = 8.7 Hz, 2H), 7.55 (d, J = 8.5 Hz, 2H), 7.14 (d, J = 8.9 Hz, 2H), 6.47 (d, J = 6.8 Hz, 1H), 4.00 (t, J = 5.1 Hz, 4H), 3.24 (s, 4H). HRMS (ESI): found 445.12065 ($C_{20}H_{21}ClN_6O_2S$ [M + H]$^+$, requires 445.1208).

*4.2.4.6. 4-Bromo-N-(4-((2-(piperazin-1-yl)pyrimidin-4-yl)amino) phenyl) benzenesulfonamide hydrochloride (**DDO-5979**).* It was obtained in 38% yield as off-white solid; ^{1}H NMR (300 MHz, DMSO-d_6) δ 10.48 (s, 1H), 9.61 (s, 2H), 7.89 (d, J = 7.0 Hz, 1H), 7.78 (d, J = 8.7 Hz, 2H), 7.67 (d, J = 8.7 Hz, 2H), 7.56 (d, J = 8.4 Hz, 2H), 7.15 (d, J = 8.9 Hz, 2H), 6.50 (d, J = 7.0 Hz, 1H), 4.01 (t, J = 5.5 Hz, 4H), 3.25 (s, 4H). HRMS (ESI): found 491.06796 ($C_{20}H_{21}BrN_6O_2S$ [M + H]$^+$, requires 489.07028).

*4.2.4.7. N-(4-((2-(piperazin-1-yl)pyrimidin-4-yl)amino)phenyl)-4-(trifluoromethoxy) benzenesulfonamide hydrochloride (**DDO-5980**).* It was obtained in 41% yield as off-white solid; ^{1}H NMR (300 MHz, DMSO-d_6) δ 11.05 (s, 0H), 10.53 (s, 1H), 9.59 (s, 1H), 7.89 (d, J = 8.1 Hz, 2H), 7.57 (d, J = 8.3 Hz, 3H), 7.16 (d, J = 8.9 Hz, 1H), 6.49 (d, J = 7.0 Hz, 1H), 4.01 (d, J = 5.1 Hz, 4H), 3.24 (s, 4H). HRMS (ESI): found 495.14170 ($C_{21}H_{21}F_3N_6O_3S$ [M + H]+, requires 495.14207).

*4.2.4.8. N-(4-((2-(piperazin-1-yl)pyrimidin-4-yl)amino)phenyl)-[1,1′-biphenyl]-4-sulfonamide hydrochloride (**DDO-5981**).* It was obtained in 40% yield as off-white solid; ^{1}H NMR (300 MHz, DMSO-d_6) δ 9.17 (s, 1H), 7.93 (d, J = 5.6 Hz, 1H), 7.91−7.81 (m, 4H), 7.79−7.70 (m, 2H), 7.58−7.43 (m, 5H), 7.10 (d, J = 8.7 Hz, 2H), 6.01 (d, J = 5.7 Hz, 1H), 3.64 (t, J = 5.1 Hz, 4H), 2.78 (t, J = 5.0 Hz, 4H). HRMS (ESI): found487.19082 ($C_{26}H_{26}N_6O_2S$ [M + H]$^+$, requires 487.19107).

*4.2.4.9. N-(4-((2-(piperazin-1-yl)pyrimidin-4-yl)amino)phenyl)-4-propylbenzenesulfonamide hydrochloride (**DDO-5982**).* It was obtained in 39% yield as off-white solid; ^{1}H NMR (300 MHz, DMSO-d_6) δ 9.14 (s, 1H), 7.88 (d, J = 5.7 Hz, 1H), 7.62 (d, J = 8.1 Hz, 2H), 7.47 (d, J = 8.9 Hz, 2H), 7.33 (d, J = 8.1 Hz, 2H), 6.99 (d, J = 8.9 Hz, 2H), 5.96 (d, J = 5.7 Hz, 1H), 3.58 (t, J = 4.8 Hz, 4H), 2.72 (t, J = 4.9 Hz, 4H), 2.57 (t, J = 7.6 Hz, 2H), 1.56 (h, J = 7.4 Hz, 2H), 0.84 (t, J = 7.3 Hz, 3H). HRMS (ESI): found 453.20688 ($C_{23}H_{28}N_6O_2S$ [M + H]$^+$, requires 453.20672).

*4.2.4.10. 4-Phenoxy-N-(4-((2-(piperazin-1-yl)pyrimidin-4-yl)amino) phenyl) benzenesulfonamide hydrochloride (**DDO-5983**).* It was obtained in 33% yield as off-white solid; ^{1}H NMR (300 MHz, DMSO-d_6) δ 9.15 (s, 1H), 7.87 (d, J = 5.6 Hz, 1H), 7.70 (d, J = 8.9 Hz, 2H), 7.53−7.37 (m, 4H), 7.23 (t, J = 7.4 Hz, 1H), 7.11−6.97 (m, 6H), 5.95 (d, J = 5.6 Hz, 1H), 3.58 (t, J = 4.9 Hz, 4H), 2.71 (t, J = 5.0 Hz, 4H). HRMS (ESI): found 221.05887 ($C_{26}H_{26}N_6O_3S$ [M + H]$^+$, requires 221.05885).

*4.2.4.11. 4-(benzyloxy)-N-(4-((2-(piperazin-1-yl)pyrimidin-4-yl) amino)phenyl) benzenesulfonamide hydrochloride (**DDO-5984**).* It was obtained in 34% yield as off-white solid; ^{1}H NMR (300 MHz, DMSO-d_6) δ 9.13 (s, 1H), 7.88 (d, J = 5.6 Hz, 1H), 7.64 (d, J = 8.9 Hz, 2H), 7.53−7.28 (m, 7H), 7.12 (d, J = 8.9 Hz, 2H), 6.99 (d, J = 8.9 Hz, 2H), 5.95 (d, J = 5.7 Hz, 1H), 5.13 (s, 2H), 3.58 (t, J = 5.0 Hz, 4H), 2.71 (t, J = 5.0 Hz, 4H). HRMS (ESI): found 517.20129($C_{27}H_{28}N_6O_3S$ [M + H]$^+$, requires 517.20164).

*4.2.4.12. 4-Methyl-N-(4-((2-(piperazin-1-yl)pyrimidin-4-yl)amino) phenyl) benzenesulfonamide hydrochloride (**DDO-5985**).* It was obtained in 35% yield as off-white solid; ^{1}H NMR (300 MHz, DMSO-d_6) δ 11.02 (s, 1H), 10.31 (s, 1H), 9.59 (s, 2H), 7.88 (d, J = 7.0 Hz, 1H), 7.71−7.56 (m, 2H), 7.52 (d, J = 8.5 Hz, 2H), 7.34 (d, J = 8.1 Hz, 2H), 7.22−7.03 (m, 2H), 6.48 (d, J = 7.0 Hz, 1H), 4.00 (t, J = 5.3 Hz, 4H), 3.24 (s, 4H), 2.33 (s, 3H). HRMS (ESI): found 425.17507 ($C_{21}H_{24}N_6O_2S$ [M + H]$^+$, requires 425.17542).

*4.2.4.13. 4-Ethyl-N-(4-((2-(piperazin-1-yl)pyrimidin-4-yl)amino) phenyl) benzenesulfonamide hydrochloride (**DDO-5986**).* It was obtained in 30% yield as off-white solid; ^{1}H NMR (300 MHz, DMSO-d_6) δ 11.06 (s, 1H), 10.34 (s, 1H), 9.61 (s, 2H), 7.88 (d, J = 7.1 Hz, 1H), 7.68 (d, J = 8.3 Hz, 2H), 7.54 (d, J = 8.8 Hz, 2H), 7.38 (d, J = 8.3 Hz, 2H), 7.15 (d, J = 8.9 Hz, 2H), 6.49 (d, J = 6.6 Hz, 1H), 4.01 (s, 4H), 3.24 (s, 4H), 2.64 (q, J = 7.6 Hz, 2H), 1.15 (t, J = 7.6 Hz, 3H). HRMS (ESI): found 439.19062 ($C_{22}H_{26}N_6O_2S$ [M + H]$^+$, requires 439.19107).

*4.2.4.14. 4-Isopropyl-N-(4-((2-(piperazin-1-yl)pyrimidin-4-yl) amino)phenyl) benzenesulfonamide hydrochloride (**DDO-5987**).* It was obtained in 37% yield as off-white solid; ^{1}H NMR (300 MHz, DMSO-d_6) δ 11.08 (s, 0H), 10.38 (s, 1H), 9.64 (s, 2H), 7.90 (d, J = 7.0 Hz, 1H), 7.72 (d, J = 8.3 Hz, 2H), 7.57 (d, J = 8.5 Hz, 2H), 7.44 (d, J = 8.3 Hz, 2H), 7.19 (d, J = 8.9 Hz, 2H), 6.51 (d, J = 7.0 Hz, 1H), 4.04 (t, J = 5.1 Hz, 4H), 3.27 (s, 4H), 2.96 (p, J = 6.8 Hz, 1H), 1.20 (d, J = 6.9 Hz, 6H). HRMS (ESI): found 453.20629 ($C_{23}H_{28}N_6O_2S$ [M + H]$^+$, requires 453.20672).

*4.2.4.15. 4-Butyl-N-(4-((2-(piperazin-1-yl)pyrimidin-4-yl)amino) phenyl) benzenesulfonamide hydrochloride (**DDO-5988**).* It was obtained in 39% yield as off-white solid; ^{1}H NMR (300 MHz, DMSO-d_6) δ 9.16 (s, 1H), 7.93 (d, J = 5.6 Hz, 1H), 7.67 (d, J = 8.1 Hz, 2H), 7.51 (d, J = 8.8 Hz, 2H), 7.38 (d, J = 8.1 Hz, 2H), 7.04 (d, J = 8.8 Hz, 2H), 6.00 (d, J = 5.6 Hz, 1H), 3.63 (t, J = 4.9 Hz, 4H), 2.76 (t, J = 4.9 Hz, 4H), 2.65 (t, J = 7.7 Hz, 2H), 1.66−1.49 (m, 2H), 1.36−1.26 (m, 2H), 0.91 (t, J = 7.3 Hz, 3H). HRMS (ESI): found 467.22212 ($C_{24}H_{30}N_6O_2S$ [M + H]$^+$, requires 467.22237).

*4.2.4.16. 4-Pentyl-N-(4-((2-(piperazin-1-yl)pyrimidin-4-yl)amino) phenyl) benzenesulfonamide hydrochloride (**DDO-5989**).* It was obtained in 32% yield as off-white solid; ^{1}H NMR (300 MHz, DMSO-d_6) δ 11.02 (s, 1H), 10.32 (s, 1H), 9.60 (s, 2H), 7.88 (d, J = 7.0 Hz, 1H), 7.69−7.63 (m, 2H), 7.53 (d, J = 8.6 Hz, 2H), 7.39−7.33 (m, 2H), 7.18−7.10 (m, 2H), 6.48 (d, J = 6.9 Hz, 1H), 4.01 (t, J = 4.9 Hz, 4H), 3.23 (t, J = 8.2 Hz, 4H), 2.60 (t, 2H), 1.66−1.44 (m, 2H), 1.29−1.19 (m, 4H), 0.83 (t, J = 6.9 Hz, 3H). HRMS (ESI): found 481.23766 ($C_{25}H_{32}N_6O_2S$ [M + H]$^+$, requires 481.23802).

*4.2.4.17. Ethyl 4-(N-(4-((2-(piperazin-1-yl)pyrimidin-4-yl)amino) phenyl)sulfamoyl) benzoate hydrochloride (**DDO-5990**).* It was obtained in 34% yield as off-white solid; ^{1}H NMR (300 MHz, DMSO-d_6) δ 9.17 (s, 1H), 8.08 (d, J = 8.0 Hz, 2H), 7.89 (d, J = 5.7 Hz, 1H), 7.84 (d, J = 8.1 Hz, 2H), 7.47 (d, J = 8.5 Hz, 2H), 6.99 (d, J = 8.4 Hz, 2H), 5.98 (d, J = 5.7 Hz, 1H), 4.33 (q, J = 7.1 Hz, 2H), 3.62 (t, J = 5.0 Hz, 4H), 2.78 (t, J = 4.9 Hz, 4H), 1.32 (t, J = 7.2 Hz, 3H). HRMS (ESI): found 483.18073 ($C_{23}H_{26}N_6O_4S$ [M + H]$^+$, requires 483.18090).

*4.2.4.18. 2,4,6-Triisopropyl-N-(4-((2-(piperazin-1-yl)pyrimidin-4-yl) amino)phenyl) benzenesulfonamide hydrochloride (**DDO-5991**).* It was obtained in 40% yield as off-white solid; ^{1}H NMR (300 MHz, DMSO-d_6) δ 9.15 (s, 1H), 7.87 (d, J = 5.6 Hz, 1H), 7.48 (d, J = 8.7 Hz, 2H), 7.19 (s, 2H), 6.95 (d, J = 8.6 Hz, 2H), 5.94 (d, J = 5.7 Hz, 1H), 3.57 (t, J = 4.9 Hz, 4H), 2.70 (t, J = 5.3 Hz, 4H), 1.17 (d, J = 6.9 Hz, 6H), 1.12

(d, J = 6.7 Hz, 12H). HRMS (ESI): found 537.30023 ($C_{29}H_{40}N_6O_2S$ $[M + H]^+$, requires 537.30062).

*4.2.4.19. N-(4-((2-(piperazin-1-yl)pyrimidin-4-yl)amino)phenyl)-2,3-dihydrobenzofuran-5-sulfonamide hydrochloride (**DDO-5992**).* It was obtained in 37% yield as off-white solid; ^{1}H NMR (300 MHz, DMSO-d_6) δ 9.10 (s, 1H), 7.88 (d, J = 5.6 Hz, 1H), 7.58 (s, 1H), 7.49 (d, J = 2.3 Hz, 1H), 7.48−7.42 (m, 2H), 7.01 (d, J = 9.0 Hz, 2H), 6.85 (d, J = 8.4 Hz, 1H), 5.96 (d, J = 5.6 Hz, 1H), 4.60 (t, J = 8.8 Hz, 2H), 3.60 (t, J = 5.0 Hz, 4H), 3.20 (t, J = 8.7 Hz, 2H), 2.73 (t, 4H). HRMS (ESI): found 453.17072 ($C_{22}H_{24}N_6O_3S$ $[M + H]^+$, requires 453.17034).

*4.2.4.20. N-(4-((2-(piperazin-1-yl)pyrimidin-4-yl)amino)phenyl)-2,3-dihydro-1H-indene-5-sulfonamide hydrochloride (**DDO-5993**).* It was obtained in 35% yield as off-white solid; ^{1}H NMR (300 MHz, DMSO-d_6) δ 9.10 (s, 1H), 7.87 (d, J = 5.6 Hz, 1H), 7.57 (s, 1H), 7.47 (t, J = 9.5 Hz, 3H), 7.34 (d, J = 7.9 Hz, 1H), 7.01 (d, J = 8.8 Hz, 2H), 5.95 (d, J = 5.7 Hz, 1H), 3.58 (t, J = 5.0 Hz, 4H), 2.87 (t, J = 7.4 Hz, 4H), 2.72 (t, J = 5.1 Hz, 4H), 2.09−1.96 (m, 2H). HRMS (ESI): found 451.19085 ($C_{23}H_{26}N_6O_2S$ $[M + H]^+$, requires 451.19107).

*4.2.4.21. 2,2,4,6,7-Pentamethyl-N-(4-((2-(piperazin-1-yl)pyrimidin-4-yl)amino)phenyl)-2,3-dihydrobenzofuran-5-sulfonamide hydrochloride (**DDO-5994**).* It was obtained in 42% yield as off-white solid; ^{1}H NMR (300 MHz, DMSO-d_6) δ 11.10 (s, 0H), 10.10 (s, 1H), 9.65 (s, 2H), 7.87 (d, J = 7.0 Hz, 1H), 7.52 (d, J = 8.4 Hz, 2H), 7.21−6.99 (m, 2H), 6.50 (d, J = 6.8 Hz, 1H), 4.02 (s, 4H), 3.24 (s, 4H), 2.98 (s, 2H), 2.47 (s, 3H), 2.40 (s, 3H), 2.01 (s, 3H), 1.40 (s, 6H). ^{13}C NMR (75 MHz, DMSO-d_6) δ 170.85, 161.25, 160.75, 159.22, 156.28, 139.29, 136.90, 134.12, 132.12, 129.37, 125.57, 121.77, 120.65, 117.35, 97.83, 87.38, 60.25, 49.05, 43.60, 42.69, 41.93, 28.62, 21.23, 19.67, 17.93, 14.53, 12.80. HRMS (ESI): found 523.24844 ($C_{27}H_{34}N_6O_3S$ $[M + H]^+$, requires 523.24859).

4.3. Biological assays and computational studies

4.3.1. Cloning, expression, and purification of recombinant Hsp90 and Cdc37

The process of cloning, expression, and purification of recombinant Hsp90 and Cdc37 was performed as a similar procedure as previous reported [35].

4.3.2. Biolayer interferometry assay

The process of biolayer interferometry assay was performed as a similar procedure as previous reported [35].

4.3.3. In vitro antiproliferative assay

Antiproliferative activities of all the compounds against HCT116 cell line were determined using an MTT assay kit. First, cells were seeded into 96-well plates at 3000−5000 cells per well and incubated for 24 h. Subsequently, serial dilutions of the compounds were added in the plates for 72 h. Then, the cell proliferation was determined by the MTT kit according to the standard protocol (Beyotime, Jiangsu, China).

4.3.4. Cellular thermal shift assay

CETSAs were performed according to previously published standard protocols [39]. HCT116 cells were seeded in 10 cm cell culture dishes to reach ~90% confluence. HCT116 cells were treated with 5 μM DDO-5994 or the same amount of DMSO before they were collected and washed with PBS buffer three times. The collected cells were isolated and resuspended in PBS buffer, which were equally distributed into 200 μL PCR tubes. The tubes were heated at the indicated temperature (37−75 °C) to denature the samples for 3 min. Subsequently, the denatured cells were freeze-thawed three times in liquid nitrogen before being centrifuged and analyzed by Western blot.

4.3.5. Co-IP assay

HCT116 cells were seeded in 10 cm cell culture dishes to reach ~90% confluence. Then, the cells and the indicated concentrations of compounds or the same volume of DMSO as controls were incubated together for 12 h. After being washed twice with ice cold PBS, the cells were lysed by radio-immunoprecipitation assay (RIPA) buffer (50 mM Tris, 150 mM NaCl, 1% NP-40, and protease inhibitor cocktail, Roche, pH = 7.4) for 1 h on ice, whose lysates were centrifuged at 12,000 rpm at 4 °C for 15 min. Afterward, 1 mg of cell lysates was incubated with 5 μg of *anti*-Hsp90 (sc-13119, Santa Cruz Biotechnology), *anti*-Cdc37 (4793S, Cell Signaling Technology), *anti*-CDK4 (ab199728, Abcam), or normal rabbit immunoglobulin G (IgG) (sc-2027, Santa Cruz Biotechnology) separately overnight at 4 °C on a vertical roller. Another 3 h incubation was continued after adding protein A/G Magnetic Agarose Beads (78609, Thermo Fisher Scientific) to the lysates. Lastly, the beads were washed with RIPA buffer 5 times and then subjected to SDS-PAGE, followed by Western blot analysis.

4.3.6. Cell cycle analysis

Cells treated with the indicated concentrations of DDO-5994 were incubated at 37 °C for 12 h before being harvested and fixed with 75% ethanol overnight at 4 °C. Cells were incubated with ribonuclease I (50 μg/mL) in PBS at 37 °C for 30 min, and stained by PI (50 μg/mL) for 15 min. Cell cycle assays were performed on Flow cytometry and FACSDiva software, v6.2 (BD Biosciences). FlowJo software was used to analyze the cell cycle phases.

4.3.7. Cell culture

HCT116 cell lines were obtained from the Cell Resource Center of Shanghai Institute for Biological Sciences, Chinese Academy of Sciences. The cell lines used in this study were maintained in RPMI 1640 medium supplemented with 10% fetal bovine serum. All the cells were authenticated by short tandem repeat profiling, examined for mycoplasma contamination, and cultured at 37 °C in a humidified, 5% CO_2 containing atmosphere incubator (Thermo Fisher Scientific).

4.3.8. Tumor xenograft experiments

HCT116 cells (1×10^7) and Matrigel (BD Biosciences) were mixed together in a 3:1 vol on ice and injected into the flanks of 6-week-old BALB/c nude mice which were randomly divided into three groups to generate xenografts. The treatment began when the mean tumor volumes reached 125 mm^3, and continued for 37 days, giving an oral administration of 0.9% saline solution containing 5% DMSO (vehicle) and compounds (**DDO-5994** and **18h**, 10 or 20 mg/kg) daily. By measuring the two perpendicular diameters of the tumors, the tumor volume was determined everyday (V = length (mm) × width (mm)^2/2), and the body weights were recorded every 1−4 days. After 37 days, the mice were sacrificed and dissected, whose tumor tissues and experimental organs were weighed and collected for further study. All animals used in this study were handled according to federal and institutional guidelines under a protocol approved by the Institutional Animal Care and Use Committee at China Pharmaceutical University.

4.3.9. H&E staining and immunohistochemistry

The process of H&E staining and immunohistochemistry was performed as a similar procedure as previous reported [35].

4.3.10. Statistics

GraphPad Prism 8.2.1 software was used to process

experimental data. Values are expressed in the form of mean ± SD. The data were analyzed from at least three parallel experiments. Significant differences between two groups were indicated as $*P < 0.05$, $**P < 0.01$, and $***P < 0.001$.

4.3.11. Molecular docking and molecular dynamics (MD) simulation

The crystal structure of Hsp90-Cdc37 (PDB ID: 1US7) was obtained from the Protein Data Bank (PDB). All the compounds and protein structures were imported to Discovery Studio (DS) 4.0 for molecular docking. Conformations' generation of protein and compounds were performed by "Prepare Protein" and "Prepare Ligands" protocol, respectively. The protein residues involving Hsp90-Cdc37 PPI predominantly (including Glu47 and Gln133) were defined as the binding sites. Molecular Docking was performed using the LibDock tool with default parameters unless otherwise mentioned. The MD simulation and analysis of MD trajectories were carried out as a similar procedure as previous reported [34].

Author contributions

The manuscript was written through contributions of all authors. All authors have given approval to the final version of the manuscript.

Declaration of competing interest

The authors declare that they have no known competing financial interests or personal relationships that could have appeared to influence the work reported in this paper.

Acknowledgments

This study was supported by projects 82003582, 81872737, 81773639 and 81930100 of the National Natural Science Foundation of China; BK20190559 of the Natural Science Foundation of Jiangsu Province of China; CPU2018GY02 of the Double First Class Innovation Team of China Pharmaceutical University; the National Science & Technology Major Project "Key New Drug Creation and Manufacturing Program", China (No: 2018ZX09711002, 2017ZX09302003 and 2015ZX09101032); the Project Program of State Key Laboratory of Natural Medicines, China Pharmaceutical University(No. SKLNMZZ202003 and No. SKLNMZZ202003); the Priority Academic Program Development of Jiangsu Higher Education Institutions.

Appendix A. Supplementary data

Supplementary data to this article can be found online at https://doi.org/10.1016/j.ejmech.2020.112959.

References

[1] L. Whitesell, S.L. Lindquist, HSP90 and the chaperoning of cancer, Nat. Rev. Canc. 5 (2005) 761–772.
[2] M. Taipale, D.F. Jarosz, S. Lindquist, HSP90 at the hub of protein homeostasis: emerging mechanistic insights, Nat. Rev. Mol. Cell Biol. 11 (2010) 515–528.
[3] M.M. Biebl, J. Buchner, Structure, function, and regulation of the Hsp90 machinery, Cold Spring Harb. Perspect. Biol. 11 (2019).
[4] M. Taipale, I. Krykbaeva, M. Koeva, C. Kayatekin, K.D. Westover, G.I. Karras, S. Lindquist, Quantitative analysis of HSP90-client interactions reveals principles of substrate recognition, Cell 150 (2012) 987–1001.
[5] L. Stepanova, X. Leng, S.B. Parker, J.W. Harper, Mammalian p50Cdc37 is a protein kinase-targeting subunit of Hsp90 that binds and stabilizes Cdk4, Genes Dev. 10 (1996) 1491–1502.
[6] Y. Kimura, S.L. Rutherford, Y. Miyata, I. Yahara, B.C. Freeman, L. Yue, R.I. Morimoto, S. L, Cdc37 is a molecular chaperone with specific functions in signal transduction, Genes Dev. 11 (1997) 1775–1785.
[7] N. Grammatikakis, J.H. Lin, A. Grammatikakis, P.N. Tsichlis, B.H. Cochran, p50(cdc37) acting in concert with Hsp90 is required for Raf-1 function, Mol. Cell Biol. 19 (1999) 1661–1672.
[8] T. Hunter, R.Y. Poon, Cdc37: a protein kinase chaperone? Trends Cell Biol. 7 (1997) 157–161.
[9] R. Conde, J. Xavier, C. McLoughlin, M. Chinkers, N. Ovsenek, Protein phosphatase 5 is a negative modulator of heat shock factor 1, J. Biol. Chem. 280 (2005) 28989–28996.
[10] J. Oberoi, D.M. Dunn, M.R. Woodford, L. Mariotti, J. Schulman, D. Bourboulia, M. Mollapour, C.K. Vaughan, Structural and functional basis of protein phosphatase 5 substrate specificity, Proc. Natl. Acad. Sci. U. S. A. 113 (2016) 9009–9014.
[11] R.A. Sager, N. Dushukyan, M. Woodford, M. Mollapour, Structure and function of the co-chaperone protein phosphatase 5 in cancer, Cell Stress & Chaperones 25 (2020) 383–394.
[12] M.E. Murphy, The HSP70 family and cancer, Carcinogenesis 34 (2013) 1181–1188.
[13] S.M. Doyle, J.R. Hoskins, A.N. Kravats, A.L. Heffner, S. Garikapati, S. Wickner, Intermolecular interactions between Hsp90 and Hsp70, J. Mol. Biol. 431 (2019) 2729–2746.
[14] J. Li, K. Richter, J. Reinstein, J. Buchner, Integration of the accelerator Aha1 in the Hsp90 co-chaperone cycle, Nat. Struct. Mol. Biol. 20 (2013) 326–331.
[15] J.R. Smith, P.A. Clarke, E. de Billy, P. Workman, Silencing the cochaperone CDC37 destabilizes kinase clients and sensitizes cancer cells to HSP90 inhibitors, Oncogene 28 (2009) 157–169.
[16] A.K. Mandal, P. Lee, J.A. Chen, N. Nillegoda, A. Heller, S. DiStasio, H. Oen, J. Victor, D.M. Nair, J.L. Brodsky, A.J. Caplan, Cdc37 has distinct roles in protein kinase quality control that protect nascent chains from degradation and promote posttranslational maturation, J. Cell Biol. 176 (2007) 319–328.
[17] P.J. Gray, T. Prince, J. Cheng, M.A. Stevenson, S.K. Calderwood, Targeting the oncogene and kinome chaperone CDC37, Nat. Rev. Canc. 8 (2008) 491–495.
[18] Y.L. Janin, ATPase inhibitors of heat-shock protein 90, second season, Drug Discov. Today 15 (2010) 342–353.
[19] L. Neckers, P. Workman, Hsp90 molecular chaperone inhibitors: are we there yet? Clin. Canc. Res. 18 (2012) 64–76.
[20] C.E. Stebbins, A.A. Russo, C. Schneider, N. Rosen, F.U. Hartl, N.P. Pavletich, Crystal structure of an Hsp90-geldanamycin complex: targeting of a protein chaperone by an antitumor agent, Cell 89 (1997) 239–250.
[21] Y.S. Kim, S.V. Alarcon, S. Lee, M.J. Lee, G. Giaccone, L. Neckers, J.B. Trepel, Update on Hsp90 inhibitors in clinical trial, Curr. Top. Med. Chem. 9 (2009) 1479–1492.
[22] R. Garcia-Carbonero, A. Carnero, L. Paz-Ares, Inhibition of HSP90 molecular chaperones: moving into the clinic, Lancet Oncol. 14 (2013) E358–E369.
[23] L. Li, L. Wang, Q.D. You, X.L. Xu, Heat shock protein 90 inhibitors: an update on achievements, challenges, and future directions, J. Med. Chem. 63 (2020) 1798–1822.
[24] L. Wang, L. Li, Z.H. Zhou, Z.Y. Jiang, Q.D. You, X.L. Xu, Structure-based virtual screening and optimization of modulators targeting Hsp90-Cdc37 interaction, Eur. J. Med. Chem. 136 (2017) 63–73.
[25] L. Wang, L. Li, K. Gu, X.L. Xu, Y. Sun, Q.D. Y, Targeting hsp90-cdc37: a promising therapeutic strategy by inhibiting Hsp90 chaperone function, Curr. Drug Targets 18 (2017) 1572–1585.
[26] L. Wang, L. Li, W.T. Fu, Z.Y. Jiang, Q.D. You, X.L. Xu, Optimization and bioevaluation of Cdc37-derived peptides: an insight into Hsp90-Cdc37 protein-protein interaction modulators, Bioorg. Med. Chem. 25 (2017) 233–240.
[27] S. Sreeramulu, S.L. Gande, M. Gobel, H. Schwalbe, Molecular mechanism of inhibition of the human protein complex Hsp90-Cdc37, a kinome chaperone-cochaperone, by triterpene celastrol, Angew Chem. Int. Ed. Engl. 48 (2009) 5853–5855.
[28] N. Li, M. Xu, B. Wang, Z. Shi, Z. Zhao, Y. Tang, X. Wang, J. Sun, L. Chen, Discovery of novel celastrol derivatives as hsp90–cdc37 interaction disruptors with antitumor activity, J. Med. Chem. 62 (2019) 10798–10815.
[29] W. Huang, Q.D. Wu, M. Zhang, Y.L. Kong, P.R. Cao, W. Zheng, J.H. Xu, M. Ye, Novel Hsp90 inhibitor FW-04-806 displays potent antitumor effects in HER2-positive breast cancer cells as a single agent or in combination with lapatinib, Canc. Lett. 356 (2015) 862–871.
[30] Y. Yu, A. Hamza, T. Zhang, M. Gu, P. Zou, B. Newman, Y. Li, A.A. Gunatilaka, C.G. Zhan, D. Sun, Withaferin A targets heat shock protein 90 in pancreatic cancer cells, Biochem. Pharmacol. 79 (2010) 542–551.
[31] D. Li, C. Li, L. Li, S. Chen, L. Wang, Q. Li, X. Wang, X. Lei, Z. Shen, Natural product Kongensin A is a non-canonical HSP90 inhibitor that blocks RIP3-dependent necroptosis, Cell Chem Biol 23 (2016) 257–266.
[32] S.M. Roe, M.M. Ali, P. Meyer, C.K. Vaughan, B. Panaretou, P.W. Piper, C. Prodromou, L.H. Pearl, The Mechanism of Hsp90 regulation by the protein kinase-specific cochaperone p50(cdc37), Cell 116 (2004) 87–98.
[33] X. Chen, P. Liu, Q. Wang, Y. Li, L. Fu, H. Fu, J. Zhu, Z. Chen, W. Zhu, C. Xie, L. Lou, DCZ3112, a novel Hsp90 inhibitor, exerts potent antitumor activity against HER2-positive breast cancer through disruption of Hsp90-Cdc37 interaction, Canc. Lett. 434 (2018) 70–80.
[34] L. Wang, L.X. Zhang, L. Li, J.S. Jiang, Z. Zheng, J.L. Shang, C.X. Wang, W.L. Chen, Q.C. Bao, X.L. Xu, Z.Y. Jiang, J. Zhang, Q.D. You, Small-molecule inhibitor targeting the Hsp90-Cdc37 protein-protein interaction in colorectal cancer, Sci. Adv. 5 (2019), eaax2277.
[35] L. Wang, J.S. Jiang, L.X. Zhang, Q.Y. Zhang, J.R. Zhou, L. Li, X.L. Xu, Q.D. You, Discovery and optimization of small molecules targeting the protein-protein

interaction of heat shock protein 90 (Hsp90) and cell division cycle 37 as orally active inhibitors for the treatment of colorectal cancer, J. Med. Chem. 63 (2020) 1281–1297.
[36] K.A. Verba, R.Y. Wang, A. Arakawa, Y. Liu, M. Shirouzu, S. Yokoyama, D.A. Agard, Atomic structure of Hsp90-Cdc37-Cdk4 reveals that Hsp90 traps and stabilizes an unfolded kinase, Science 352 (2016) 1542–1547.
[37] L. Lamphere, F. Fiore, X. Xu, L. Brizuela, S. Keezer, C. Sardet, G.F. Draetta, J. Gyuris, Interaction between Cdc37 and Cdk4 in human cells, Oncogene 14 (1997) 1999–2004.
[38] J.R. Smith, E. de Billy, S. Hobbs, M. Powers, C. Prodromou, L. Pearl, P.A. Clarke, P. Workman, Restricting direct interaction of CDC37 with HSP90 does not compromise chaperoning of client proteins, Oncogene 34 (2015) 15–26.
[39] D. Martinez Molina, R. Jafari, M. Ignatushchenko, T. Seki, E.A. Larsson, C. Dan, L. Sreekumar, Y. Cao, P. Nordlund, Monitoring drug target engagement in cells and tissues using the cellular thermal shift assay, Science 341 (2013) 84–87.